



**HAL**  
open science

## Small signal analysis of DC voltage control based on a virtual resistance of DC/DC converter integrated in a multiterminal DC grid

Ghazala Shafique, Johan Boukhenfouf, Francois Gruson, Shabab Samimi, Frédéric Colas, Xavier Guillaud

### ► To cite this version:

Ghazala Shafique, Johan Boukhenfouf, Francois Gruson, Shabab Samimi, Frédéric Colas, et al.. Small signal analysis of DC voltage control based on a virtual resistance of DC/DC converter integrated in a multiterminal DC grid. IET Generation, Transmission & Distribution, 2024, pp.1-14. 10.1049/gtd2.13262 . hal-04695980

**HAL Id: hal-04695980**

**<https://hal.science/hal-04695980v1>**


Submitted on 12 Sep 2024

**HAL** is a multi-disciplinary open access archive for the deposit and dissemination of scientific research documents, whether they are published or not. The documents may come from teaching and research institutions in France or abroad, or from public or private research centers.

L'archive ouverte pluridisciplinaire **HAL**, est destinée au dépôt et à la diffusion de documents scientifiques de niveau recherche, publiés ou non, émanant des établissements d'enseignement et de recherche français ou étrangers, des laboratoires publics ou privés.

## ORIGINAL RESEARCH

# Small signal analysis of DC voltage control based on a virtual resistance of DC/DC converter integrated in a multiterminal DC grid

Ghazala Shafique<sup>1</sup>  | Johan Boukhenfouf<sup>1</sup> | François Gruson<sup>1</sup> | Shabab Samimi<sup>2</sup> | Frédéric Colas<sup>1</sup> | Xavier Guillaud<sup>1</sup>

<sup>1</sup>Univ. Lille, Arts et Metiers Institute of Technology, Centrale Lille, Junia, ULR 2697 - L2EP, Lille, France

<sup>2</sup>ESME, ESME Research Lab, Campus de Lille, Lille, France

**Correspondence**

Ghazala Shafique, Univ. Lille, Arts et Metiers Institute of Technology, Centrale Lille, Junia, ULR 2697 - L2EP, Lille, France.  
Email: ghazala.shafique@ensam.eu

This paper is a preprint of a paper submitted to the IET Generation, Transmission and Distribution journal. If accepted, the copy of record will be available at IET Digital Library.

**Funding information**

Agence Nationale de la Recherche, Grant/Award Number: ANR-20-CE05-0034 DICIT

**Abstract**

The future multi-terminal direct-current (MTDC) grid will require the interconnection of point-to-point high-voltage (HV) DC links with different specifications such as DC voltage level, system grounding configuration and HVDC technology. To adapt these differences, it is obligatory for DC/DC converters to interconnect HVDC links. Additionally, they are capable of providing supplementary functionalities as they are highly controllable devices. In this article, a primary virtual resistance DC voltage controller associated with DC/DC converter is proposed for managing DC grid voltages of the interconnected HVDC grids, increasing the reliability of the system. The commonly known topology, Front-to-Front Modular Multilevel Converter (F2F-MMC) is adopted for DC/DC converter. Time-domain simulations are performed using EMTP software for validating the controller behaviour under power disturbances and large events of loss of one converter in a MMC-based MTDC system. The converters are modelled using reduced order modelling (ROM) methodology. Apart from this, dynamic studies have been carried out using a linear state space model for small-signal stability analysis of a HVDC system integrating DC/DC converter with a virtual resistance DC voltage controller. The results are examined through parametric sensitivity analysis.

## 1 | INTRODUCTION

With the rising need for the utilization of renewable energy, HVDC transmission has been recognised as the best solution for long-distance bulk power transfer. The most common HVDC systems are point-to-point (P2P) schemes, connecting an individual converter directly to another through a DC cable or line. Multiterminal DC (MTDC) schemes have emerged to be more advantageous for HVDC transmission as they offer more reliability, flexibility, and balanced and coordinated power dispatch. Nowadays, MTDC systems are gaining more interest and few are already in operation while some projects are under study [1]. With the benefits of the MTDC grid, soon, a meshed HVDC system would increase interconnecting more than one terminal. Further, several MTDC networks could aggregate and form a DC grid, which could eventually evolve and result in

global or local DC Supergrid [2]. In the future and for creating a flexible DC grid, instead of creating new MTDC networks, the more reliable and practical option is to interconnect the existing P2P links. To date, the HVDC system does not have an established standard characteristic and so its installation properties vary from project to project. The independent P2P links can have different voltage levels, technologies (Line-commutated converter LCC, Voltage source converter VSC) and grounding characteristics (bipolar, monopolar) depending upon the installation features. Therefore, to adapt these differences, DC/DC converters are mandatory as an intermediate component [3, 4].

Over the last few years, the focus on the study of DC/DC converter for HVDC grids has increased. Many studies have been proposed in literature discussing the different topologies, control and validation of operation of DC/DC converter in the MTDC grid [5–10]. Some application scenarios of integrating

This is an open access article under the terms of the [Creative Commons Attribution-NonCommercial-NoDerivs](https://creativecommons.org/licenses/by-nc-nd/4.0/) License, which permits use and distribution in any medium, provided the original work is properly cited, the use is non-commercial and no modifications or adaptations are made.

© 2024 The Author(s). *IET Generation, Transmission & Distribution* published by John Wiley & Sons Ltd on behalf of The Institution of Engineering and Technology.

DC/DC converter in HVDC grid has also been investigated. Reference [11] discusses the interconnection of HVDC links with different grounding schemes. Reference [12] presents the case where a DC/DC converter is used for the interconnection of LCC and VSC-based HVDC links. Besides working in normal operation, the fault-blocking capability and operation of DC/DC converters under DC faults have also been presented in some research studies [13–15]. Few publications have also presented the multi-port DC/DC converter topologies to connect multi-port HVDC network [16, 17]. However, in the majority of studies, DC/DC converter works with constant reference power and the additional functionality of DC/DC converter to control DC voltage has not received much attention.

One of the major aspects of the HVDC system is to ensure robust control of DC grid voltage for power flow balance [18, 19]. As of now, the DC bus voltage of an MTDC grid is controlled by the AC/DC converter. On the other hand, due to the high controllability of DC/DC converters, it has the capability to provide supplementary functionalities in addition to adapting DC grids with different characteristics. DC/DC converter could be controlled to contribute to the DC grid voltage control and so participate in the DC voltage management system. This would bring more reliability and flexibility to the MTDC grid.

Reference [20] has highlighted the operation of the DC/DC converter in power and voltage control mode. A dual droop controller has been introduced in [15] to control the DC grid voltage of both P2P networks. However, the stability effects of integrating a DC/DC converter on the HVDC system are not studied. To date in the literature, all DC voltage control possibilities have not been analysed in detail associated with DC/DC converter, which could enable the control of DC grid voltages of both interconnected grids simultaneously. Thus, in this article, a modular DC/DC converter is explored in voltage control mode and a controller is proposed interconnecting two HVDC links and contributing towards DC voltage management of both DC grids.

Moreover, the addition of a new component affects the stability of the system. So, the integration of a DC/DC converter in the HVDC system would have an impact on the stability of the MTDC network. However, this topic is yet to be explored as there are no studies in literature analysing the stability effect of integrating DC/DC converter. Therefore, a dynamic analysis has been presented in this paper based on the small-signal stability study of an MTDC system integrating a DC/DC converter. The main contributions of this paper are:

- A DC voltage controller named virtual resistance DC voltage controller similar to dual droop control is presented associated with DC/DC converter. It contributes to the DC voltage management of both DC grids simultaneously and requires tuning only one parameter. The methodology to design this parameter is proposed in this paper.
- The stability of the system is analysed on integrating a DC/DC converter through a small-signal stability analysis. Various parametric sensitivity studies have been made to present the optimal values of system parameters.

The rest of the paper is as follows. Section 2 presents in detail the idea and design of a DC/DC converter in DC voltage control mode in an MTDC network. Section 3 illustrates the modelling and control scheme employed by the components of the MTDC system. Then in Section 4, EMT simulations were carried out on the case study system, highlighting the behaviour of the DC/DC converter with a virtual resistance controller. In Section 5, a small signal stability analysis of the MTDC system integrating the DC/DC converter is presented.

## 2 | DC VOLTAGE CONTROL WITH DC/DC CONVERTER

In this section, a test case representation of the MTDC system with a DC/DC converter is presented. Then, the possibilities of DC voltage controllers linked to DC/DC converters are explored to establish an interaction between the interconnected networks in case of power disturbance. Further, the proposition of a new DC voltage controller is presented.

### 2.1 | Representation of MTDC system

The configuration of the studied MTDC system is shown in Figure 1. It consists of two DC systems with different voltage levels connected through a DC/DC converter. Each DC system is a point-to-point HVDC link with MMC technology and has a symmetric monopole configuration. The AC grid at each terminal is considered ideal and modelled with an AC voltage source with a series impedance. Front-to-Front MMC (F2F-MMC) topology is considered for DC/DC converter [13] as it is the most studied and known topology in literature.

Grid 1 is a 640 kV network formed by two stations where MMC11 is in voltage droop control mode with droop coefficient  $k_{dr1}$  and MMC12 in power control mode, connected through a cable of 300 km length. Similarly, grid 2 is a 500 kV network with two stations MMC21 (voltage droop control mode with droop coefficient  $k_{dr2}$ ) and MMC22 (power control

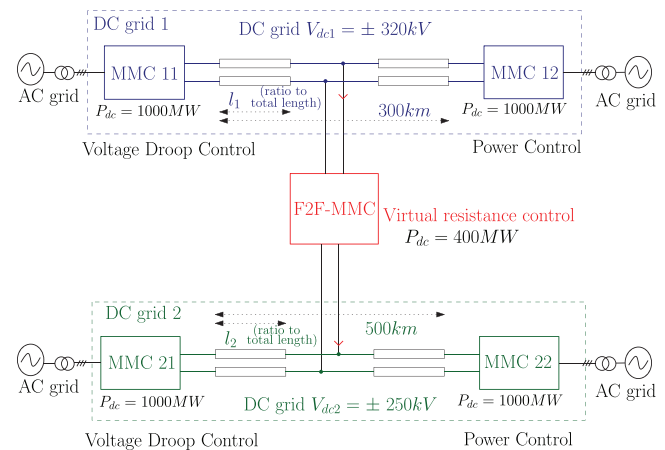


FIGURE 1 Case study MTDC system layout.

mode) connected through 500 km cable.  $l_1$  (or  $l_2$ ) is the ratio of the length between MMC11 (or MMC21) and F2F-MMC with the total length of the grid in its P2P link.

## 2.2 | DC voltage controllers possibilities

Exploring the possibility of the DC/DC converter in voltage control mode, by extending the known DC voltage controllers for VSC to DC/DC converters [18, 19]. Employing master-slave control with a DC/DC converter, will impose a power reference and thereby, making the converter work in power control mode and therefore decoupling the interconnected networks. This solution will not be considered in this work since the main objective is to propose support to DC grids. Furthermore, using the widely used DC voltage droop controller with DC/DC converter will participate in only one of the HVDC network DC voltage regulations and would not be able to support both DC grid voltages.

In addition, the droop control principle known for AC/DC converters could be extended and adapted to dual droop controller in order to control the two DC grid voltages of the interconnected network simultaneously with DC/DC converters [15]. But this type of controller would require to design two droop coefficients related to the respective DC network. Thus, in a meshed MTDC or multi-port system, the tuning and designing of coefficients would be complex to study. Unlike this approach, a similar controller is proposed in this paper named virtual resistance DC voltage controller. It simplifies the tuning process by requiring adjustment of only one parameter.

## 2.3 | Virtual resistance DC voltage controller

The main objective of the DC/DC converter is to exchange some power between the two HVDC grids. However, both HDVC networks can also provide support to each other in case of a power disturbance or if a large event occurs on one of the grids. Hence the reference power  $P_{ref}^{dc/dc}$  for the DC/DC converter can be divided into two parts as shown in Equation (1). Here,  $P_o^{dc/dc}$  is the constant nominal power of the DC/DC converter. On the other hand, the power  $\Delta P^{dc/dc}$  is associated with DC voltage support depending upon the virtual resistance controller.

$$P_{ref}^{dc/dc} = P_o^{dc/dc} + \Delta P^{dc/dc}. \quad (1)$$

The virtual resistance DC voltage controller is based on the idea of a DC/DC converter acting as a virtual resistance in series, incorporating the voltage ratio  $ntr$  as presented in Figure 2, connecting the different HVDC links. The  $ntr$  coefficient is the rated DC voltage ratio ( $V_{dc2}/V_{dc1}$ ). The control methodology is inspired by the DC voltage droop control, a method already known for the MTDC grid. The relation is given by Equations (2) and (3) and the control structure is shown in Figure 3, where the variables  $V_{dc1}$ ,  $V_{dc2}$  are the measured DC

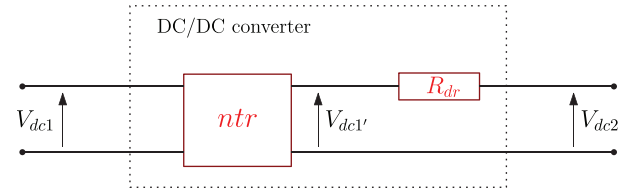


FIGURE 2 DC/DC converter representation as a virtual resistance.

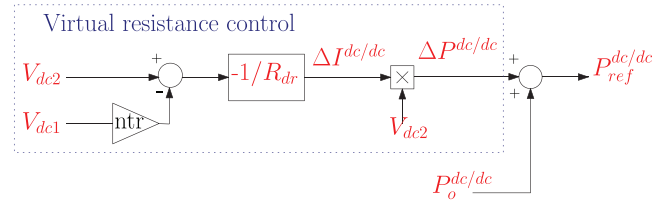


FIGURE 3 Virtual resistance DC voltage controller.

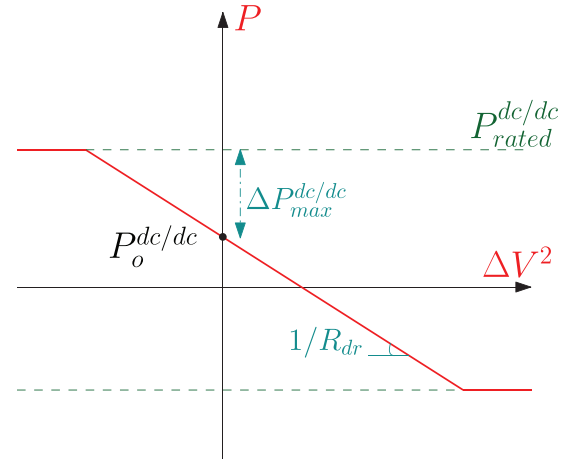


FIGURE 4  $P\Delta V^2$  characteristic with virtual resistance DC voltage controller.

grid voltages,  $R_{dr}$  is the resistance droop coefficient and  $ntr$ .

$$\Delta I^{dc/dc} = (-1/R_{dr})\Delta V^{dc/dc}, \quad (2)$$

$$\Delta P^{dc/dc} = (-1/R_{dr})(V_{dc2} - ntrV_{dc1}). \quad (3)$$

In case of any deviation in the DC grid voltages from their rated value due to the occurred power disturbance in the MTDC grids, the virtual resistance control depending on the DC voltage difference and resistance droop coefficient acts and generates the injected compensating reference  $\Delta I^{dc/dc}$ , in order to help share the power disturbance among MTDC grids. The corresponding compensating power reference  $\Delta P^{dc/dc}$  is derived as in Equation (4). Thereby, the power flow can be controlled by  $PV^2$  (power-voltage<sup>2</sup>) droop characteristic presented in Figure 4. Thus, working DC/DC converter in voltage control mode and enabling a coupling between connected grids for sharing the power disturbance and managing the DC grid voltages. Thereby, increasing the reliability and reducing the stress

of the DC system.

$$\Delta P^{dc/dc} = (-1/R_{dr})(V_{dc2}^2 - ntrV_{dc1}V_{dc2}). \quad (4)$$

## 2.4 | Resistance droop coefficient $R_{dr}$ design

The resistance droop coefficient  $R_{dr}$  can be designed using the relation in Equation (4), following the steady-state constraints on the power variation  $\Delta P^{dc/dc}$  and considering the maximum deviation of the DC grids voltages  $V_{dc2}$  and  $V_{dc1}$ .

**Step 1-** Definition of the constraint on  $\Delta P^{dc/dc}$ :

Let's consider the reference power  $P_{ref}^{dc/dc}$  equals to the maximum value, that is, equal to the rated power of DC/DC converter  $P_{rated}^{dc/dc}$ . Now using Equation (1), the maximum change in DC/DC converter power  $\Delta P_{max}^{dc/dc}$ , related to its rated power  $P_{rated}^{dc/dc}$  and nominal power  $P_o^{dc/dc}$  is as given by Equation (5).  $\pm$  sign is related to the direction of power flow.

$$\Delta P_{max}^{dc/dc} = \pm P_{rated}^{dc/dc} - P_o^{dc/dc} \quad (5)$$

**Step 2-** Definition of the constraint on  $V_{dc2}$  and  $V_{dc1}$ :

To consider the constraints, the DC grid voltages are written as given in Equation (6), where  $V_{dc1_n}$ ,  $V_{dc2_n}$  are the nominal voltages and  $\Delta v_{dc1_{max}}$ ,  $\Delta v_{dc2_{max}}$  are their respective maximum voltage deviation. Usually, the acceptable voltage deviation limit is considered as  $\pm 5\%$ . Also, individual local DC voltage controllers are implemented at both DC grids; therefore, the deviation of  $V_{dc1}$  and  $V_{dc2}$  will also depend on their respective DC voltage controller methodology.

$$\begin{aligned} V_{dc1} &= V_{dc1_n} - \Delta v_{dc1_{max}}, \\ V_{dc2} &= V_{dc2_n} - \Delta v_{dc2_{max}}. \end{aligned} \quad (6)$$

Now, to have the maximum constraint, the worst-case scenario is considered, where only one AC/DC converter (MMC) out of the four is controlling the DC voltage. In this scenario, the whole burden of DC power imbalance of both grids will fall on one converter. Two cases have to be considered depending upon which converter is controlling the DC voltage.

**Case 1:** Considering DC voltage droop controller to be present only at DC grid 1, that is, at converter station MMC11. Whereas, considering no DC voltage controller to be present at DC grid 2. So only MMC11 has the ability to compensate the power disturbance. Now, in case of power disturbance at DC grid 2, the disturbance will be compensated by sharing the power from DC grid 1 (MMC11) through a DC/DC converter with the virtual resistance controller.

The power disturbance is considered as the maximum power change possible for DC/DC converter  $\Delta P_{max}^{dc/dc}$ . Since this whole power disturbance is compensated by MMC11 (with droop coefficient  $k_{dr1}$ ), then the DC grid 1 voltage deviation  $\Delta v_{dc1_{max}}$  would be given by Equation (7). Now, the  $R_{dr}$  is designed such that the DC grid 2 voltage deviation  $\Delta v_{dc2_{max}}$  is under the

maximum DC voltage deviation limit of  $\pm 5\%$ .

$$\text{Case 1 : } \Delta v_{dc1_{max}} = -k_{dr1}(-\Delta P_{max}^{dc/dc}). \quad (7)$$

**Case 2:** Similar to case 1, considering DC voltage droop controller only at DC grid 2 (MMC21) and no voltage controller at DC grid 1. So, any power disturbance on DC grid 1 will be compensated by DC grid 2 (MMC21 with droop coefficient  $k_{dr2}$ ) through DC/DC converter. Thus, the voltage deviation  $\Delta v_{dc2_{max}}$  can be given by Equation (8).  $R_{dr}$  is designed to limit  $\Delta v_{dc1_{max}}$  to  $\pm 5\%$  deviation limit.

$$\text{Case 2 : } \Delta v_{dc2_{max}} = -k_{dr2}\Delta P_{max}^{dc/dc}. \quad (8)$$

**Step 3-** Calculating  $R_{dr}$ : Rewriting Equation (4) and considering the constraint on  $\Delta P^{dc/dc}$ ,  $R_{dr}$  is presented by Equation (9).  $R_{dr}$  is calculated considering the above cases and the constraints given by Equations (5)–(8). Thus, for case 1 and case 2,  $R_{dr1}$  and  $R_{dr2}$  are calculated as presented by Equations (10) and (11), respectively. The best suitable value of  $R_{dr}$  for a given MTDC system is the minimum value obtained in the calculation (Equation 12), in order to satisfy all the constraints simultaneously. Here, the value of  $R_{dr}$  changes with the operating point of the DC/DC converter ( $P_o^{dc/dc}$ ) and system parameters ( $k_{dr1}$ ,  $k_{dr2}$ ) and so it has to be updated following a change in the system specification.

$$R_{dr} = \left| \frac{(V_{dc2}^2 - ntrV_{dc1}V_{dc2})}{\Delta P_{max}^{dc/dc}} \right|. \quad (9)$$

$$\text{Case 1 : } R_{dr1} = \left| \frac{(V_{dc2_n} \pm 5\%)^2 - ntrV_{dc1}(V_{dc2_n} \pm 5\%)}{\pm P_{rated}^{dc/dc} - P_o^{dc/dc}} \right|, \quad (10)$$

where,

$$V_{dc1} = V_{dc1_n} - (k_{dr1}\Delta P_{max}^{dc/dc}).$$

$$\text{Case 2 : } R_{dr2} = \left| \frac{V_{dc2}^2 - ntr(V_{dc1_n} \pm 5\%)V_{dc2}}{\pm P_{rated}^{dc/dc} - P_o^{dc/dc}} \right|, \quad (11)$$

where,

$$V_{dc2} = V_{dc2_n} - (k_{dr2}\Delta P_{max}^{dc/dc}),$$

$$R_{dr} = \min(R_{dr1}, R_{dr2}). \quad (12)$$

## 2.5 | Numerical illustration of designing the resistance droop coefficient $R_{dr}$

In this section, the numerical calculation of  $R_{dr}$  is presented, considering the MTDC test case shown in Figure 1.



### Step 1- Constraint on $\Delta P^{dc/dc}$ :

Considering  $P_o^{dc/dc}$  as 200 MW and  $P_{rated}^{dc/dc}$  as 400 MW, Equation (5) gives,

$$\Delta P_{max}^{dc/dc} = [-600 \text{ MW} \quad 200 \text{ MW}] \quad (13)$$

### Step 2- Constraint on $V_{dc2}$ and $V_{dc1}$ :

The nominal DC voltages are:  $V_{dc1_n} = 640 \text{ kV}$  and  $V_{dc2_n} = 500 \text{ kV}$ .

**Case 1:** Let the DC voltage droop controller to be present only at DC grid 1, at converter station MMC11 with droop coefficient:  $k_{dr1} = 3.2e - 5$  (0.05 p.u.). Using Equations (13) and (7), the deviation in  $V_{dc1}$  is given by:

$$\Delta v_{dc1_{max}} = [-19200 \text{ V} \quad 6400 \text{ V}] \quad (14)$$

Thus, from Equation (6),  $V_{dc1}$  is calculated as below,

$$V_{dc1} = [659.2 \text{ kV} \quad 633.6 \text{ kV}] \quad (15)$$

Now, the  $R_{dr}$  is designed such that the DC grid 2 voltage deviation  $\Delta v_{dc2_{max}}$  is under the limit of  $\pm 5\%$ , that is

$$\Delta v_{dc2_{max}} = 500 \text{ kV} (\pm 5\%). \quad (16)$$

So, from Equation (6),  $V_{dc2}$  is calculated as:

$$V_{dc2} = [525 \text{ kV} \quad 475 \text{ kV}]. \quad (17)$$

**Case 2:** In this case, the DC voltage droop controller is considered to be present only at DC grid 2, at converter station MMC21 with droop coefficient:  $k_{dr1} = 2.5e - 5$  (0.05 p.u.). So, from Equations (13) and (8), the deviation in  $V_{dc2}$  is given by:

$$\Delta v_{dc2_{max}} = [15000 \text{ V} \quad -5000 \text{ V}]. \quad (18)$$

From Equation (6),  $V_{dc2}$  is calculated as:

$$V_{dc2} = [485 \text{ kV} \quad 505 \text{ kV}] \quad (19)$$

Now, the  $R_{dr}$  is designed such that the DC grid 1 voltage deviation  $\Delta v_{dc1_{max}}$  is under the limit of  $\pm 5\%$ , that is

$$\Delta v_{dc1_{max}} = 640 \text{ kV} (\pm 5\%) \quad (20)$$

So, from Equation (6),  $V_{dc1}$  is calculated as:

$$V_{dc1} = [608 \text{ kV} \quad 672 \text{ kV}] \quad (21)$$

### Step 3- Calculating $R_{dr}$ :

For case1, from the value of constraints  $\Delta P_{max}^{dc/dc}$ ,  $V_{dc1}$  and  $V_{dc2}$  obtained as given in Equations (13), (15) and (17), respectively, the  $R_{dr1}$  is given using Equation (10) as:

$$R_{dr1} = [8.7 \quad 47.5]. \quad (22)$$

Similarly, for case 2, using the values obtained in Equations (13), (19) and (21), the  $R_{dr2}$  is given using the Equation (11)

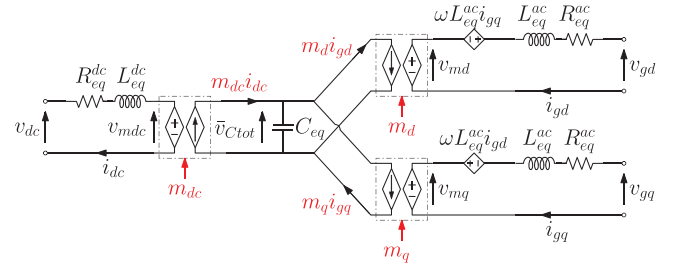


FIGURE 5 MMC reduced order model.

as:

$$R_{dr2} = [8.0833 \quad 50.5]. \quad (23)$$

At last, as presented in Equation (12), the minimum value of  $R_{dr}$  is selected to meet all the constraints simultaneously, that is

$$R_{dr} = 8.0833. \quad (24)$$

## 3 | MODELLING AND CONTROL OF THE SYSTEM COMPONENTS

In this section, the modelling and control methodologies adopted for different components (converters and cables) of the MTDC system are discussed. The studied MTDC system (Figure 1) consists of 4 MMC converters, a F2F-MMC converter and DC cables.

### 3.1 | Modular multilevel converter (MMC)

MMCs are modelled with a Reduced Order Model (ROM) methodology suitable for large-scale dynamic studies and small signal stability analysis as presented in [21]. This model is derived from an average-arm model with the assumption of well-achieved low-level control of MMC, that is, it is considered that the internal energy of the sub-modules (SMs) capacitor are balanced and there are no circulating currents in the arms. The ROM model reduces the number of state variables in the system and preserves the average internal dynamic behavior of the MMC. The MMC ROM circuit is presented in Figure 5 [21].

The control structure of the MMC ROM is illustrated in Figure 6. The control of AC and DC side is decoupled. The inner loops consists of AC currents ( $i_{gd}$ ,  $i_{gq}$ ) and DC current ( $i_{dc}$ ) controllers. The reference for DC current ( $i_{dc,ref}$ ) is provided by the output of energy stored control loop controlling the total energy stored in capacitor ( $W_{tot}$ ). In order to help in DC bus voltage dynamics, the reference for  $W_{tot,ref}$  is associated with DC voltage  $v_{dc}$  [22]. The  $i_{gd,ref}$  depends on AC power reference  $P_{ac,ref}$  which further depends on the MMC control mode, that is, controlling the power transfer or the DC grid voltage. In our case study, MMC11 and MMC21 are in voltage control mode using DC voltage droop control whereas, MMC12 and MMC22 are in active power control mode. The voltage droop coefficient  $k_{dr1}$  and  $k_{dr2}$  for MMC11 and MMC21, respectively,

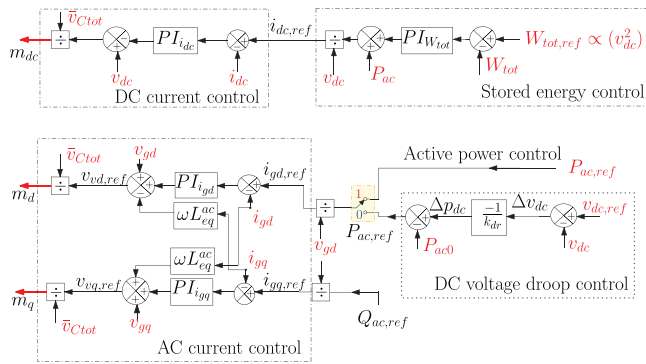


FIGURE 6 MMC ROM control scheme.

are computed depending on the usual condition of maximum 5% voltage deviation for a 1 p.u. power change [19].

### 3.2 | Front-to-front MMC (F2F-MMC)

The ROM model of the F2F-MMC can be deduced using the same approximation as with MMC. The structure is similar to cascading two ROM MMC models, front to front with a transformer on AC side as presented in Figure 7. The internal energy stored ( $W_{tot1}$ ,  $W_{tot2}$ ) and DC currents ( $i_{dc1}$ ,  $i_{dc2}$ ) of both MMC is independently controlled same as the DC side control of MMC as discussed previously. Whereas, the AC current is controlled differently as both sides are coupled with transformer and there is no external AC grid.

Thus, the adopted control scheme is presented in [13, 23], where one MMC of the DC/DC converter fixes its AC voltage and the other MMC is responsible for power flow, thereby,

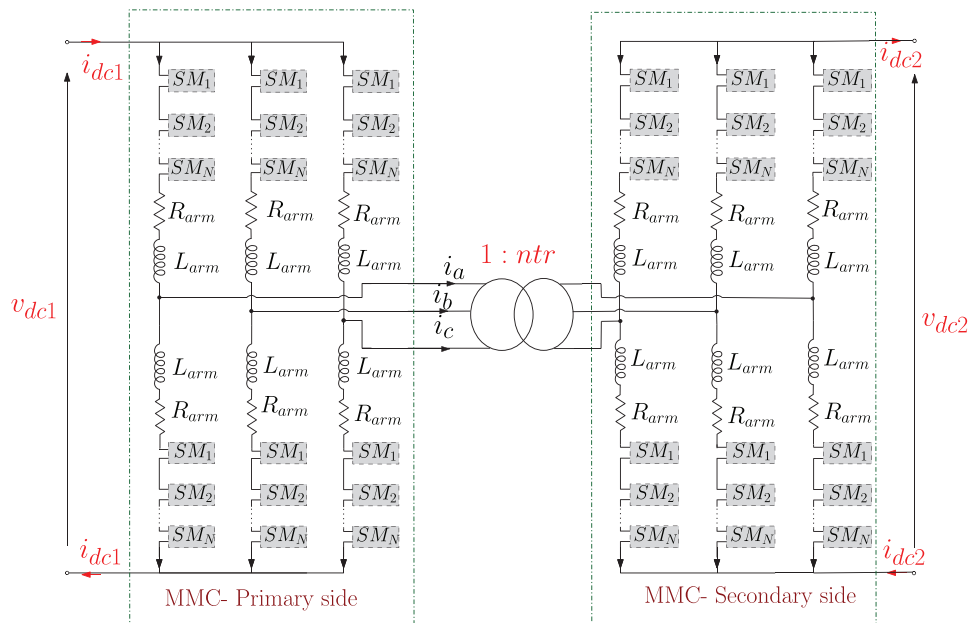


FIGURE 7 F2F-MMC structure.

controlling the AC current. The AC voltage of the primary side MMC of DC/DC converter (connected to DC grid 1) is fixed to the value  $v_{dc1}/2$ , which is the optimal operating point [24]. The secondary side MMC (connected to DC grid 2) controls the AC current. F2F-MMC will be working in voltage control mode and so the power reference  $P_{ref}^{dc/dc}$  is given related to the output of virtual resistance DC voltage control.

### 3.3 | DC cable

To exhibit accurate dynamics in transient analysis and small signal stability analysis of an HVDC power system, the frequency-dependent behaviour of cable parameters is necessary to include in the cable modelling. The best-known model is the Wide-Band (WB) model, but their conversion into a state space form required for small signal stability analysis (SSSA) cannot be directly obtained. The most commonly used model for these studies is a simple pi-line model but they do not take into account the frequency dependency behaviour [25]. Thus, for EMT simulation, WB model is used in our study. But for SSSA, an alternative pi-model with multiple parallel branches is used proposed by [26], which accurately exhibits the frequency-dependent behaviour of the cable up to the desired frequency range. The parameters of the FDPI cable model [26] are calculated using a vector-fitting approximation of the frequency-dependent series impedance of the cable. This model has been validated with the Wide-Band model in EMTP software in the frequency domain. It exhibits the same behaviour up to the first resonance cut-off frequency of the cable using one pi-section and three parallel branches, that is, for 10 km cable length the model is validated up to 4 kHz frequency.

**TABLE 1** System parameters.

Parameter	Values
$v_{dc1}$	640 kV
$v_{dc2}$	500 kV
Voltage ratio $1/ntr$	1.28
Length of DC grid 1	300 km
Length of DC grid 2	500 km
Position of F2F-MMC $l_1, l_2$	0.5
$k_{dr1}$	0.05 p.u.
$k_{dr2}$	0.05 p.u.
$P_{rated}^{dc/dc}$	$\pm 400$ MW
$R_{dr}$	8.0833 $\Omega$

## 4 | INFLUENCE OF VIRTUAL RESISTANCE CONTROLLER ON THE DYNAMIC BEHAVIOR OF MTDC SYSTEM WITH DC/DC CONVERTER IN CASE OF EVENTS

Electro-Magnetic Transient simulation (EMT) of the study case system (presented in above section) is carried out using EMTP software [27]. In order to observe the behaviour of virtual resistance controller, different scenarios are introduced in the system and the resulting DC powers and DC voltages are studied.

### 4.1 | System parameters

The test case MTDC system presented in Figure 1 is considered and the parameters are given in Table 1. Other detailed parameters are given in Appendix. The resistance droop coefficient  $R_{dr}$  is calculated using the design method discussed in section 2 and depending on the HVDC systems parameters and constraints, that is, DC grid voltages, MMC DC voltage droop coefficients ( $k_{dr1}, k_{dr2}$ ) and DC/DC converter rated power ( $P_{rated}^{dc/dc}$ ).

### 4.2 | System under power disturbance

In this section, the system is studied under power disturbances at the DC grids. A change in power set point at station MMC12 and MMC22 are introduced and the resulting DC voltages are compared between the case where DC/DC converter works with and without the virtual resistance controller. The DC power flowing from a MMC station is represented with a negative sign whereas the power coming into the MMC station is represented with a positive sign.

#### 4.2.1 | Case 1: Disturbance at DC grid 1

At  $t = 0.5$  s, a power disturbance is introduced in DC grid 1 with an increase of 140 MW (0.14 p.u.) power at station MMC12. The resulting DC power and DC voltages are shown

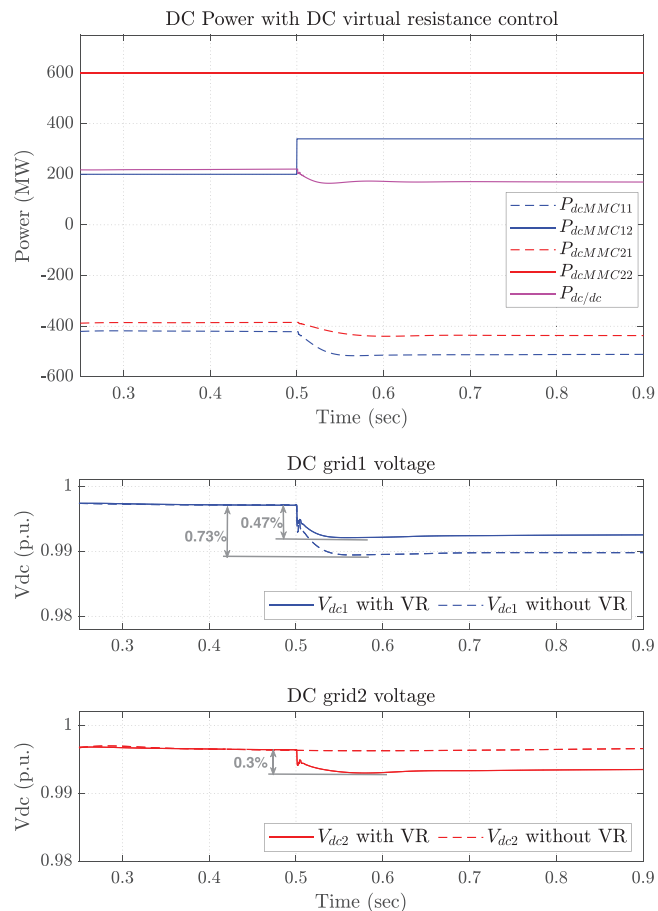


**FIGURE 8** Case 1: Power disturbance at station MMC12. Variation of DC power (at MMC11, MMC12, MMC21, MMC22, F2F-MMC) and DC grid voltages with and without virtual resistance (VR) controller.

in Figure 8. In the case where DC/DC converter is in power control mode, that is, without the virtual resistance controller, the whole disturbance is compensated by the voltage droop-controlled station MMC11 at DC grid 1 with a change of DC voltage of 0.73%. There is no effect on DC grid 2, that is, both DC grids are decoupled. Whereas, in the case with virtual resistance (VR) controller, a change in power is observed at station MMC11 (DC grid 1) as well as at voltage droop-controlled station MMC21 of DC grid 2, in order to compensate the power imbalance at MMC12 and maintaining the DC grid voltage of both grids under 5% limit. Here, the power disturbance is shared between two stations, resulting in a lesser change in DC voltage of 0.47% at DC grid 1 and a slight DC voltage deviation of 0.3% at DC grid 2. The power at F2F-MMC is not constant and it changes according to the shared power from the DC grid 2, thus establishing a link between the interconnected grids.

#### 4.2.2 | Case 2: Disturbance at DC grid 2

At  $t = 0.6$  s, a 100 MW (0.1 p.u.) change of power is introduced at station MMC22 of DC grid 2 and the results are presented in Figure 9. With virtual resistance controller, similar to case1, the power disturbance is compensated by voltage droop controlled



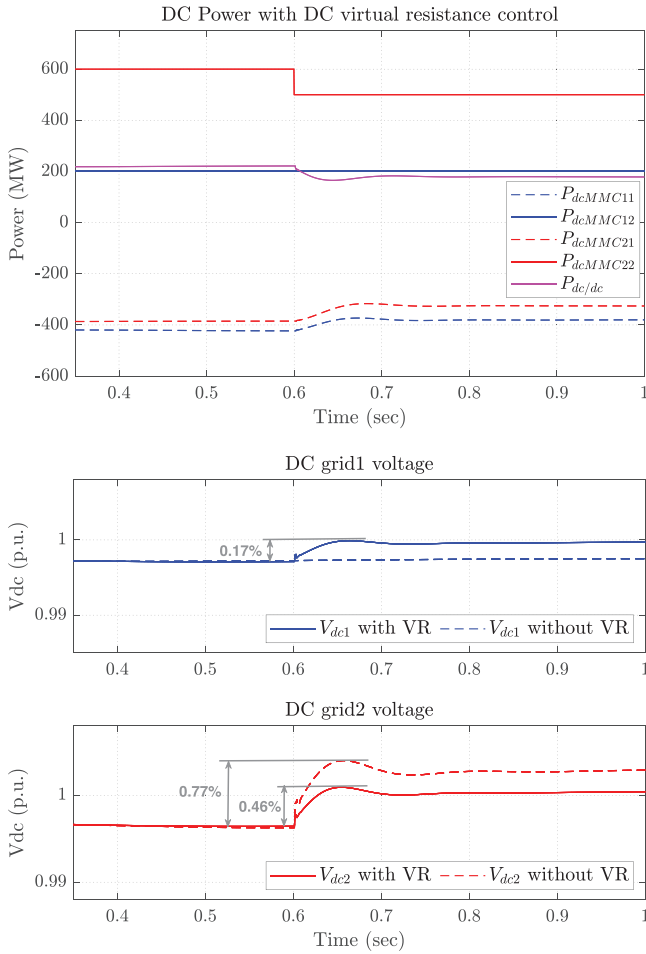


**FIGURE 9** Case 2: Power disturbance at station MMC22. Variation of DC power (at MMC11, MMC12, MMC21, MMC22, F2F-MMC) and DC grid voltages with and without virtual resistance (VR) controller.

station MMC21 (DC grid 2) and station MMC11 of DC grid 1 to regulate the DC voltages. Resulting a change in the exchanged power between the two DC grids through F2F-MMC station. As a consequence, the observed DC voltage sag (0.46%) at DC grid 2 is less compared to the voltage sag of 0.77% without the virtual resistance control.

Therefore, sharing of the power disturbance among the interconnected grids validates the behaviour of virtual resistance controller. In both cases, as the system operates with voltage droop controllers, the DC voltages have a steady state error depending on the droop coefficients ( $k_{dr1}$ ,  $k_{dr2}$ ,  $R_{dr}$ ). Also, the behaviour of the power and voltages of the MMC's and F2F-MMC are observed to be smooth with no high oscillations or abrupt transient periods.

### 4.3 | Tripping of a voltage-controlled MMC station

In this part, the behaviour of the system under a large disturbance is observed. At  $t = 0.7$  s, there is a sudden loss of MMC11 (voltage droop control) station from the MTDC system and the

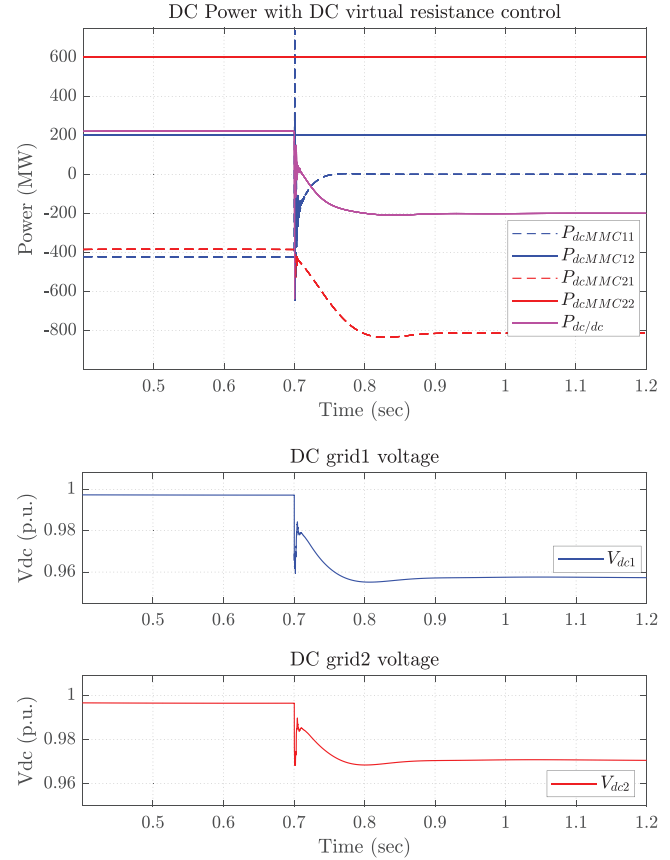


**FIGURE 10** With tripping of station MMC11: Variation of DC power (at MMC11, MMC12, MMC21, MMC22, F2F-MMC) and DC grid voltages.

resulting DC power and DC voltages are shown in Figure 10. At DC grid 1, there is no more power coming from MMC11 station whereas MMC12 is still in constant power mode with the same power reference, as a result, DC grid 1 voltage  $v_{dc1}$  should start to decrease. But with the virtual resistance controller, as both DC grids are coupled through F2F-MMC, the virtual resistance acts in order to manage the DC voltages. Consequently, MMC21 station starts to change its power to balance the power flow. Thus, following a small transient, in steady state the DC power of the remaining MTDC system is balanced and the DC voltages are under their constrained values. DC power of F2F-MMC station is now flowing from DC grid 2 to DC grid 1. On the other hand, in this case, if operating without a virtual resistance DC voltage controller at F2F-MMC, could have an adverse effect. As it would result in a continuous decrease in voltage  $v_{dc1}$  because of the absence of a voltage-controlled station to manage the power flow in DC grid 1.

Through the above results, it can be concluded that with the help of the virtual resistance controller with an F2F-MMC converter, a link can be established between MTDC grids of different specifications. It is not only possible to have DC systems to exchange desired power flow but also the functionality to participate in sharing the power disturbance between different grids for the management of DC grid voltages. Thereby, reducing the stress in DC voltage management and making the MTDC system more reliable.

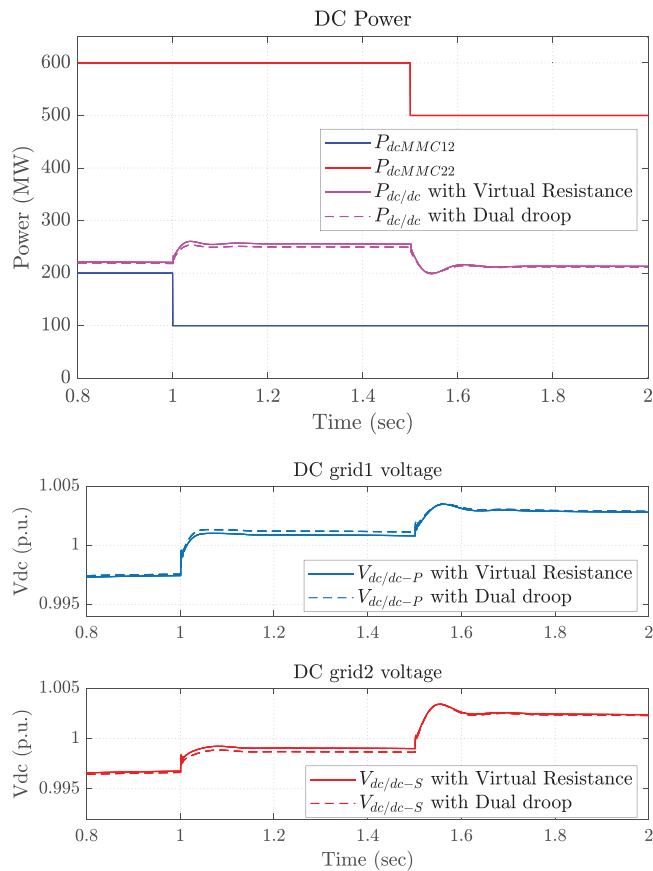


**FIGURE 11** Comparative result between virtual resistance and dual droop control: Variation of DC power (at MMC12, MMC22, F2F-MMC) and DC grid voltages.

#### 4.4 | Comparison between virtual resistance and dual droop controller

In this section, the behaviour of virtual resistance control is compared with another possible DC voltage control, that is, the dual droop control (with dual droop coefficients as 0.05 p.u.). The power at station MMC12 and MMC22 is decreased by 100 MW (0.1 p.u.) at  $t = 1$  s and  $t = 1.5$  s, respectively. The comparative results are presented in Figure 11. As can be observed, the voltage and power waveform have similar dynamic behaviour with the two controllers. The disturbances in the system are being shared by the interconnected grids and the DC grid voltages are controlled within their specified limits. The major difference is in the steady state values and static behaviour, which is due to the difference in the designed coefficient values of the controllers.

Thus, it can be concluded that the virtual resistance controller and dual droop controller have similar dynamic characteristics with a small steady state difference. But the advantage of the virtual resistance controller is the need to tune only one coefficient whereas with dual droop controller two droop coefficients need to be optimized. Therefore, dual droop design would be complex for a meshed MTDC system. On the other hand, the

virtual resistance DC voltage controller is largely simpler to implement.

## 5 | SMALL SIGNAL STABILITY ANALYSIS (SSSA) OF MTDC SYSTEM INTEGRATING DC/DC CONVERTER

In the preceding section, the dynamic behaviour of the MTDC system, which integrates the DC/DC converter and the DC voltage controller, was explored through time domain analysis. Additionally, further analysis is needed to investigate how changes in various parameters of the MTDC system impact its stability.

The models of MTDC system components used for EMT analysis above are non-linear and has to be linearised for small signal stability analysis. Therefore, the first part of this section addresses the linearisation of the MTDC system and validates the linear model by comparing it with the nonlinear EMT model. Subsequently, several parametric sensitivity analyses are conducted to assess how different system parameters influence the system's stability.

### 5.1 | Linearised MTDC system model

The HVDC system is composed of different subsystems—MMCs, F2F-MMC converter and DC cables. The converters are further divided into subsystems of physical models and control systems. The linear state space model of the complete MTDC system is computed using the association of the linearised model of its different subsystems. The linearisation and small signal modelling approach utilized in this paper are detailed in the first chapter of the reference [28]. Additionally, the association principle is discussed in Appendix B of the same reference.

The linear time-invariant (LTI) model of reduced order model (ROM) MMC is composed of AC and DC side physical parts, along with its controllers (current and stored energy control loop). The detailed linearisation model of MMC can be found in [29, 30]. Apart from this, the models of the MMC11 and MMC21 converter include the DC voltage droop control loop [29]. As previously mentioned, the F2F-MMC converter consists of two MMCs connected front to front and the ROM of F2F-MMC is two times the ROM MMC connected to the DQ side (factoring in the transformer ratio gain). Thus, the LTI model of ROM F2F-MMC model is derived using the same methodology as for the MMC and includes a virtual resistance DC voltage control loop. The DC grid cables are modelled with the FDPI model with three parallel branches and DC bus capacitance at each station node. The linearized state space model for DC grid cables (FDPI model) is presented in [31].

The MTDC system with its subsystems representing the global inputs of each subsystem is presented in Figure 12. The individual state variables ( $x$ ) of each subsystem are shown in

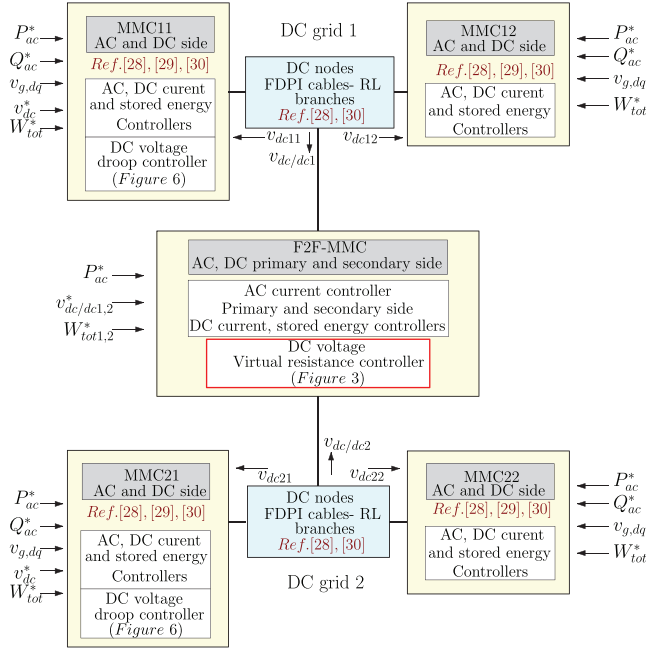


FIGURE 12 Subsystem representation of MTDC system.

Equation (25).

$$\begin{aligned}
 \mathbf{x}_{MMC} &= \underbrace{[i_{g,dq} \ i_{dc} \ v_{c,tot}]}_{\text{physical part}} \underbrace{[\xi_{i_{g,dq}} \ \xi_{i_{dc}} \ \xi_{W_{tot}}]}_{\text{controllers}} \\
 \mathbf{x}_{F2F-MMC} &= \underbrace{[i_{g,dq} \ i_{dc1} \ i_{dc2} \ v_{c,tot1} \ v_{c,tot2}]}_{\text{physical part}} \underbrace{[\xi_{i_{g,dq}} \ \xi_{i_{dc1}} \ \xi_{i_{dc2}} \ \xi_{W_{tot1}} \ \xi_{W_{tot2}}]}_{\text{Controllers}} \\
 \mathbf{x}_{FDPI} &= \underbrace{[v_{dc11} \ v_{dc12} \ v_{dc/dc1} \ v_{dc21} \ v_{dc22} \ v_{dc/dc2} \ \dots]}_{\text{DC bus voltage at each station node}} \\
 &\quad \dots \underbrace{[i_{L,123}^{11} \ i_{L,123}^{12} \ i_{L,123}^{21} \ i_{L,123}^{22}]}_{\text{FDPI line currents}}
 \end{aligned} \quad (25)$$

DC load flow is used to calculate the operating point DC voltages, current and powers at each station. All individual subsystems are linearised around the operating point. At last, to obtain a single state space representation of the complete MTDC system, all the subsystems are concatenated to create an aggregated model [31]. The resulting state space representation of the MTDC system is expressed by Equation (26) [32] (where  $u$  represents the inputs,  $x$  the states and  $y$  the outputs of the system,  $A, B, C, D$  are related matrices). The global input and states of the complete MTDC system are given in Equation (27).

$$\begin{aligned}
 \Delta \dot{\mathbf{x}}_{sys} &= \mathbf{A}_{sys} \Delta \mathbf{x}_{sys} + \mathbf{B}_{sys} \Delta \mathbf{u}_{sys}, \\
 \Delta \mathbf{y}_{sys} &= \mathbf{C}_{sys} \Delta \mathbf{x}_{sys} + \mathbf{D}_{sys} \Delta \mathbf{u}_{sys},
 \end{aligned} \quad (26)$$

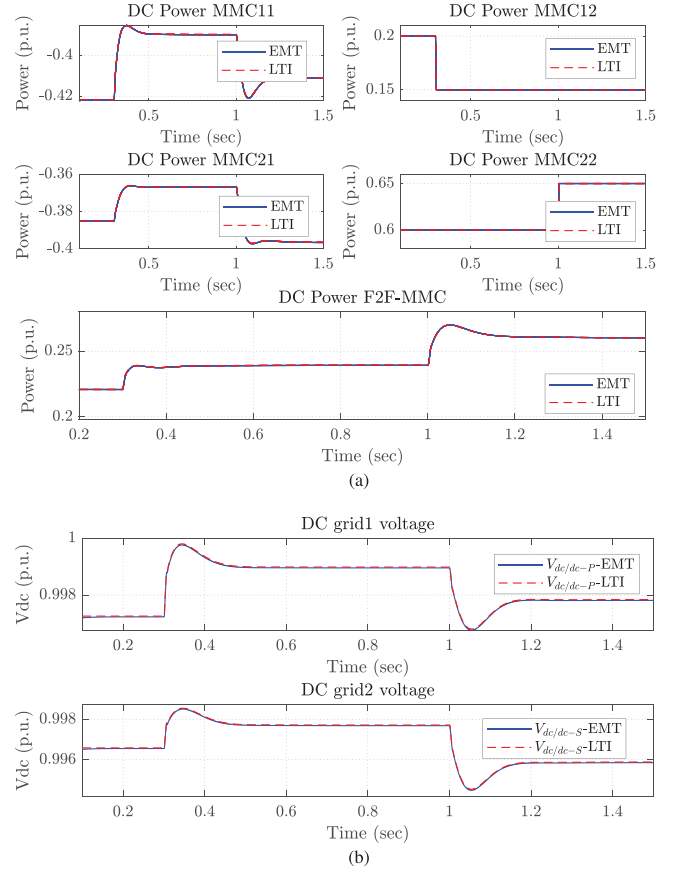


FIGURE 13 Time domain validation: (a) DC power response and (b) DC voltage response—EMT—Simulation with non-linear model, LTI—Linear time-invariant state-space model.

$$\begin{aligned}
 \mathbf{x}_{sys} &= [\mathbf{x}_{MMC11} \ \mathbf{x}_{MMC12} \ \mathbf{x}_{MMC21} \ \mathbf{x}_{MMC22} \ \dots \\
 &\quad \dots \ \mathbf{x}_{F2FMMC} \ \mathbf{x}_{FDPI}] \in \mathbb{R}^{62} \\
 \mathbf{u}_{sys} &= \underbrace{[P_{ac}^* \ v_{dc/dc1,2}^* \ W_{tot1,2}^*]}_{\text{F2F-MMC}} \underbrace{[P_{ac}^* \ Q_{ac}^* \ v_{g,dq} \ v_{dc11}^* \ W_{tot}^* \ \dots]}_{\text{MMC11}} \dots \\
 &\quad \dots \underbrace{[P_{ac}^* \ Q_{ac}^* \ v_{g,dq} \ W_{tot}^*]}_{\text{MMC21}} \underbrace{[P_{ac}^* \ Q_{ac}^* \ v_{g,dq} \ v_{dc21}^* \ W_{tot}^* \ \dots]}_{\text{MMC21}} \dots \\
 &\quad \dots \underbrace{[P_{ac}^* \ Q_{ac}^* \ v_{g,dq} \ W_{tot}^*]}_{\text{MMC22}} \in \mathbb{R}^{27}
 \end{aligned} \quad (27)$$

### 5.1.1 | Validation of linearized state space model

The small-signal model obtained has been validated using time domain simulation, comparing the obtained state space model and the non-linear model used in section IV.

The system parameters are the same as used in the previous EMT analysis. Small disturbances are introduced in the system and the comparative results are presented in Figure 13. At  $t = 0.3$  s, the power at station MMC12 (DC grid 1) is decreased by

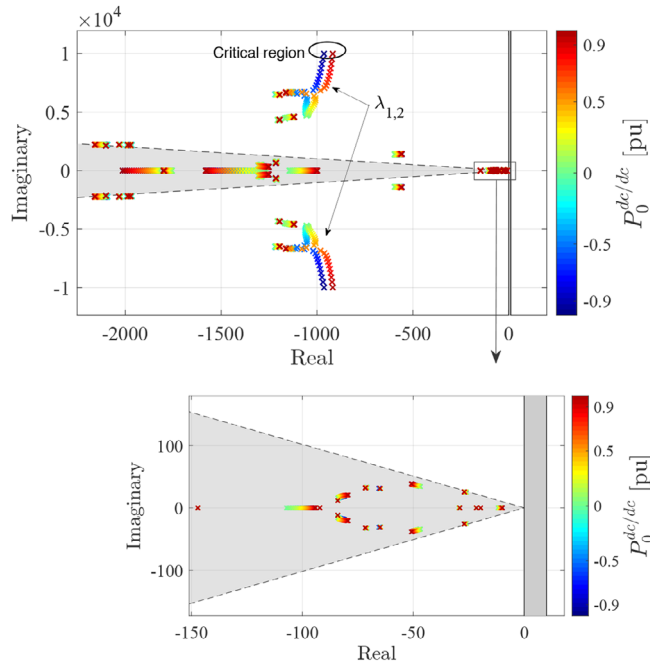


**FIGURE 14** Parametric sweep for the change of  $P_0^{dc/dc}$  to study the influence of change in  $R_{dr}$ .

0.05 p.u., as a result, MMC11 and MMC21 decrease their power in order to compensate for the power imbalance and maintain the DC voltage deviation under the limit of  $\pm 0.05$  p.u. Similarly, at  $t = 1$  s, the power at station MMC22 (DC grid 2) is increased by 0.05 p.u. and so the voltage droop control at MMC11, MMC21 and the virtual resistance control at F2F-MMC acts and compensates the power imbalance in the system.

As observed, the behaviour of DC power and DC voltages resulting from the linear state space model (LTI) follows the same dynamics as the non-linear model (EMT). Thus, the linear state space model is able to reproduce the main dynamics and overall behaviour of the MTDC system with the integration of DC/DC converter and is used for small-signal dynamics and stability analysis.

## 5.2 | Influence of $R_{dr}$

Recalling Equations (5) and (9),  $R_{dr}$  can be written as Equation (28). Here, it can be seen that the resistance droop coefficient  $R_{dr}$  depends on the operating power  $P_0^{dc/dc}$  of the DC/DC converter. So, to study the influence of the variation of  $R_{dr}$  on the stability of the system, the operating point of the converter is varied. Thus, F2F-MMC converter power  $P_0^{dc/dc}$  is varied from  $-0.9$  p.u. to  $0.9$  p.u. and the resulting eigenvalue trajectories are shown in Figure 14.

$$R_{dr} = \left| \frac{(V_{dc2}^2 - ntrV_{dc1}V_{dc2})}{\pm P_{rated}^{dc/dc} - P_0^{dc/dc}} \right|. \quad (28)$$

**TABLE 2** Eigenvalues with their dominating states and damping ratio.

$\lambda_i$	Dominating states	Critical value	Damp. ratio	Freq (Hz)
$\lambda_{1,2}$	F2FMMC $v_{dc}, i_{dc}$ of both sides	$-917.964 \pm j9978.38$	0.0916	1588.1
$\lambda_{3,4}$	MMC22 $v_{dc}, i_{dc}$	$-837.564 \pm j10155.3$	0.0822	1616.3
$\lambda_{5,6}$	MMC21 $v_{dc}, i_{dc}$	$-1029.61 \pm j14824.1$	0.0693	2359.3
$\lambda_{7,8}$	MMC12 $v_{dc}, i_{dc}$	$-670.387 \pm j12619.2$	0.053	2008.4
$\lambda_{9,10}$	MMC11 $v_{dc}, i_{dc}$	$-888.106 \pm j16561.7$	0.0535	2635.9

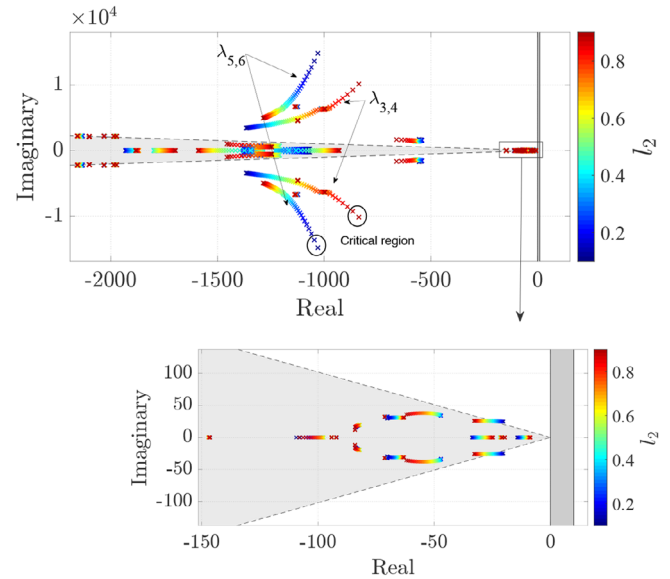


**FIGURE 15** Parametric sweep for the change of  $l_2$ .

In Figure 14, the grey region represents a high damped region with a damping ratio greater than 0.7. As can be observed, some eigenvalues do not change with operating points and they mostly correspond to the control loops of the converters. Most of the eigenvalues that are affected and vary lie in the high damped region. Eigenvalues  $\lambda_{1,2}$  corresponding to the relatively less damped regions are related to the dynamics of the DC voltage loop. Overall, the MTDC system is stable at all points. The highest participation state, that is, the dominating states corresponding to eigenvalues which are highly influenced are presented in Table 2. Moreover, the critical eigenvalue region with a low damping ratio is represented by a circle in Figure 14. The critical value for  $\lambda_{1,2}$  is  $-917.964 \pm j9978.38$  and the corresponding damping ratio and frequency of oscillations are 0.0916 and 1588.1 Hz, respectively, as presented in Table 2.

## 5.3 | Influence of positioning of DC/DC converter

In this section, the effect of the position of placing F2F-MMC in the DC grid is analysed. First,  $l_2$  (ratio of length for DC grid 2) is varied from 0.1 to 0.9 and the F2F-MMC is connected at the middle of the cable at DC grid1, that is,  $l_1 = 0.5$ . Results are shown in Figure 15, demonstrating that the dynamics of the



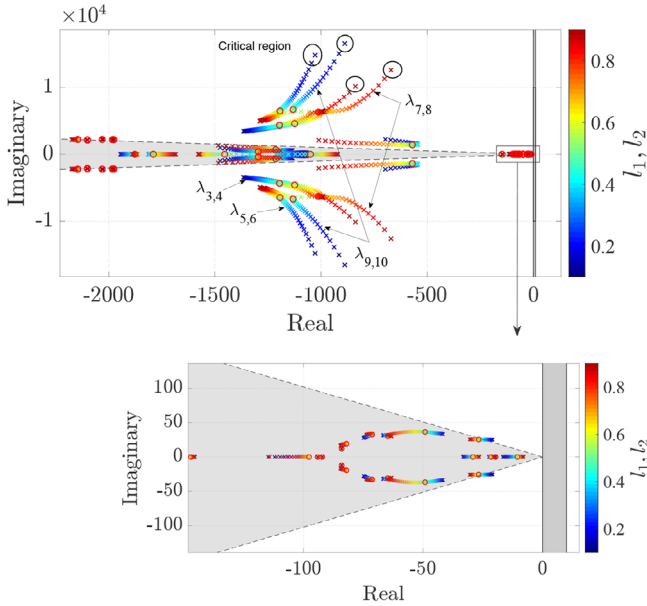


**FIGURE 16** Parametric sweep for the change of  $l_1, l_2$ .

system are impacted by the placing of the DC/DC converter on the grid. But the eigenvalues always lies in left hand side of the plane making the system stable at all places. Most of the eigenvalues lies in or near the high damped region. Eigenvalues  $\lambda_{5,6}$  related to MMC21 DC voltage and current, moves towards high damping region as  $l_2$  increases (red region), that is, the F2F-MMC converter is shifted away from MMC21 station. Whereas, eigenvalue  $\lambda_{3,4}$  related to MMC22 DC voltage and current, moves towards low damping region with increase in  $l_2$ , that is, the F2F-MMC converter is shifting towards MMC22 station.

Now,  $l_1$  and  $l_2$  both are varied from 0.1 up to 0.9 and the eigenvalues trajectories are observed as presented in Figure 16. The eigenvalues represented by a red circle correspond to the case where  $l_1, l_2 = 0.5$ . Similar to the previous case, the same behaviour was observed with the eigenvalues related to MMC stations of DC grid 1. Eigenvalue  $\lambda_{7,8}$  moves towards low damped region with F2F-MMC shifting towards MMC12 station (increasing  $l_1$ ). Whereas, Eigenvalue  $\lambda_{9,10}$  moves towards the high damped region with F2F-MMC shifting away from MMC22 station.

Therefore, it can be concluded that the MMC station connected near to F2F-MMC have more interactions between their dynamics and so exhibit comparatively less damped behaviour. While the MMC stations connected far from F2F-MMC exhibit low interactions and comparatively more damped dynamic behaviour. It can be said that the optimal region is represented by the green area in Figure 16 for overall dynamic stability of the system. The circular region on Figures 15 and 16, represents the critical region and the corresponding eigenvalue, damping ratio and frequency are given in Table 2.

## 6 | CONCLUSION

This paper has illustrated the behaviour of DC/DC converter in voltage control mode establishing a link between distinct

DC grids. A virtual resistance DC voltage controller has been proposed and compared with a dual droop controller. The control has been validated through EMT simulation of a MTDC grid with different voltage levels under the event of power disturbance and tripping of a voltage controlled MMC station. The robustness of the MTDC system integrating F2F-MMC with the virtual resistance controller has been analysed using a small-signal stability analysis. The key points to conclude are:

- It was observed that with the help of virtual resistance control, the power imbalance in one DC grid is shared and compensated by the voltage controlled converter of other DC grid through DC/DC converter. This sharing of power disturbance contributes to a reliable and flexible DC voltage management of the MTDC grid.
- The added advantage of virtual resistance controller is the requirement to tune only one parameter, unlike the dual droop controller. Thus, for a multi-port system or meshed DC system, the controller is simpler to implement.
- No instabilities were observed in the system after integrating DC/DC converter in voltage control mode. The dynamic studies have been made with different parametric analyses. It was found that the system is stable irrespective of the positioning of the F2F-MMC converter on the DC grids.

In the presented results, the MTDC system under examination has a symmetrical grounding topology. It's important to note that the virtual resistance controller is effective not only in symmetrical grounding configurations but also performs well in asymmetrical grounding setups. However, due to space limitations, additional test cases have not been presented. Further, more analysis should be done in case of DC faults in the system and with other DC/DC converter topologies. Also, the study could be expanded including the secondary control to optimise the power flow and maintain the DC voltages at their nominal values in the case of load variation.

## AUTHOR CONTRIBUTIONS

**Ghazala Shafique:** Conceptualization; data curation; formal analysis; investigation; methodology; software; validation; writing—original draft; writing—review and editing. **Johan Boukhenfouf:** Software. **François Gruson:** Conceptualization; funding acquisition; methodology; project administration; resources; supervision; writing—review and editing. **Shabab Samimi:** Software. **Frédéric Colas:** Conceptualization; methodology; supervision; writing—review and editing. **Xavier Guillaud:** Supervision; writing—review and editing.

## ACKNOWLEDGEMENTS

This work was developed during the DICIT project sponsored by a public grant overseen by the French National Research Agency as part of the “Appel à Projet Générique” (ANR-20-CE05-0034 DICIT).

## CONFLICT OF INTEREST STATEMENT

The authors declare no conflicts of interest.



## DATA AVAILABILITY STATEMENT

The data that support the findings of this study are available from the corresponding author upon reasonable request.

## ORCID

Ghazala Shafique  <https://orcid.org/0009-0008-3158-0972>

## REFERENCES

- Buigues, G., Valverde, V., Etxegarai, A., Eguía, P., Torres, E.: Present and future multiterminal HVDC systems: current status and forthcoming. *Renew. Energy Power Quality J.* 1(15), 83–88 (2017). <https://doi.org/10.24084/repqj15.223>
- Friends of Sustainable Grids: Interconnecting electricity for Europe's sustainable future. <https://supergrid.brussels/>
- Kolparambath, S.K., Suul, J.A., Tedeschi, E.: DC/DC converters for interconnecting independent HVDC systems into multiterminal DC grids. In: 2015 IEEE 13th Brazilian Power Electronics Conference and 1st Southern Power Electronics Conference (COBEP/SPEC), pp. 1–6. IEEE, Piscataway (2015)
- Gomez A, D., Paez, J.D., Cheah-Mane, M., Maneiro, J., Dworakowski, P., Gomis-Bellmunt, O., Morel, F.: Requirements for interconnection of HVDC links with DC-DC converters. In: *ECON 2019-45th Annual Conference of the IEEE Industrial Electronics Society*, pp. 4854–4860. IEEE, Piscataway (2019)
- Khan, Z.W., Minxiao, H., Kai, C., Yang, L., Rehman, A.U.: State of the art DC-DC converter topologies for the multi-terminal DC grid applications: A review. In: 2020 IEEE International Conference on Power Electronics, Smart Grid and Renewable Energy (PESGRE2020), pp. 1–7. IEEE, Piscataway (2020)
- Dworakowski, P., Paez, J.D., Frey, D., Maneiro, J., Bacha, S.: Overview of DC-DC converters dedicated to HVdc grids. *IEEE Trans. Power Delivery* 34(1), 119–128 (2019). <https://doi.org/10.1109/TPWRD.2018.2846408>
- Liang, B.Y., Li, Y.S.: A review of DC/DC converter based on MMC. In: 2017 7th International Conference on Power Electronics Systems and Applications - Smart Mobility, Power Transfer & Security (PESA), pp. 1–6. IEEE, Piscataway (2017)
- Adam, G.P., Gowaid, I.A., Finney, S.J., Holliday, D., Williams, B.W.: Review of dc-dc converters for multi-terminal HVDC transmission networks. *IET Power Electron.* 9(2), 281–296 (2016). <https://doi.org/10.1049/iet-pel.2015.0530>
- CIGRE WG. B4. 76: DC-DC converters in HVDC grids and for connections to HVDC systems (2021). <https://e-cigre.org/publication>.
- Gruson, F., Li, Y., Moigne, P.L., Delarue, P., Colas, F., Guillaud, X.: Full State Regulation of the Modular Multilevel DC Converter (M2DC) Achieving Minimization of Circulating Currents. *IEEE Trans. Power Delivery* 35(1), 301–309 (2020). <https://doi.org/10.1109/TPWRD.2019.2942527>
- Gomez D, Shinoda K, Alvarez J.P, et al.: Case study of dc-MMC interconnecting two HVDC lines with different grid topologies. In: *CIGRE Symposium*. IEEE, Piscataway (2021)
- Ahmed, K.H., Alsokhry, F., Ashraf, M., Nazih, Y., Al Turki, Y., Abdel-Khalik, A.S.: A new hybrid dual active bridge modular multilevel based DC-DC converter for HVDC networks. *IEEE Access* 9, 62055–62073 (2021). <https://doi.org/10.1109/ACCESS.2021.3074543>
- Gruson, F., Tlemcani, A., Li, Y., Delarue, P., Le Moigne, P., Guillaud, X.: Model and control of the DC-DC modular multilevel converter with DC fault tolerance. *EPE J.* 30(4), 153–164 (2020). <https://doi.org/10.1080/09398368.2020.1750847>
- Páez, J.D., Maneiro, J., Frey, D., Bacha, S., Bertinato, A., Dworakowski, P.: Study of the impact of DC-DC converters on the protection strategy of HVDC grids. In: 15th IET International Conference on AC and DC Power Transmission (ACDC 2019), pp. 1–6. IET, Stevenage (2019)
- Jovicic, D., Taherbaneh, M., Taisne, J.P., Nguefeu, S.: Offshore DC grids as an interconnection of radial systems: Protection and control aspects. *IEEE Trans. Smart Grid* 6(2), 903–910 (2015). <https://doi.org/10.1109/TSG.2014.2365542>
- Kish, G.J.: On the emerging class of non-isolated modular multilevel DC-DC converters for DC and hybrid AC-DC systems. *IEEE Trans. Smart Grid* 10(2), 1762–1771 (2019). <https://doi.org/10.1109/TSG.2017.2777473>
- Adam, G.P., Alsokhry, F.: Multi-port DC-DC and DC-AC converters for large-scale integration of renewable power generation. *Sustainability* 12(20), 8440 (2020). <https://doi.org/10.3390/su12208440>
- Sayed, S.S., Massoud, A.M.: General classification and comprehensive performance assessment of multi-objective DC voltage control in multi-terminal HVDC networks. *IEEE Access* 9, 34454–34474 (2021). <https://doi.org/10.1109/ACCESS.2021.3060935>
- Rault P: Dynamic modeling and control of multi-terminal HVDC grids. Ph.D. Thesis, Laboratory of Electrical Engineering and Power Electronics (L2EP) (2014). <https://doi.org/10.1016/j.epepsr.2019.106050>
- Sun, K., Li, K.J., Wang, M., Tian, G., Wang, Z.d., Liu, Z.: Coordination control for multi-voltage-level dc grid based on the dc-dc converters. *Electr. Power Syst. Res.* 178, 106050 (2020).
- Freytes, J., Papangelis, L., Saad, H., Rault, P., Van Cutsem, T., Guillaud, X.: On the modeling of MMC for use in large scale dynamic simulations. In: 2016 Power Systems Computation Conference (PSCC), pp. 1–7. IEEE, Piscataway (2016)
- Samimi, S., Gruson, F., Delarue, P., Colas, F., Belhouane, M.M., Guillaud, X.: MMC stored energy participation to the DC bus voltage control in an HVDC link. *IEEE Trans. Power Delivery* 31(4), 1710–1718 (2016). <https://doi.org/10.1109/TPWRD.2016.2540926>
- Paez J.D.: DC-DC converters for the interconnection of HVDC grids. Ph.D. Thesis, Communauté Université Grenoble Alpes (2019)
- Vermeersch P: Contribution to the design and control of the extended overlap-alternate arm converter. Ph.D. Thesis, Laboratory of Electrical Engineering and Power Electronics (L2EP) (2021)
- Haibo, Z., Gruson, F., Florez, D., Saudemont, C.: Analysis of the influence of different cable modelling for DC series offshore wind farm. In: 2016 18th European Conference on Power Electronics and Applications (EPE'16 ECCE Europe), pp. 1–9. IEEE, Piscataway (2016)
- Beerten, J., D'Arco, S., Suul, J.A.: Frequency-dependent cable modelling for small-signal stability analysis of VSC-HVDC systems. *IET Gener. Transm. Distrib.* 10(6), 1370–1381 (2016). <https://doi.org/10.1049/iet-gtd.2015.0868>
- Mahseredjian, J., Dennetière, S., Dubé, L., Khodabakhchian, B., Gérin Lajoie, L.: On a new approach for the simulation of transients in power systems. *Electr. Power Syst. Res.* 77(11), 1514–1520 (2007). <https://doi.org/10.1016/j.epepsr.2006.08.027>
- Freytes J.: Small-signal stability analysis of modular multilevel converters and application to MMC-based multi-terminal DC grids. Ph.D. Thesis, Laboratory of Electrical Engineering and Power Electronics (L2EP) (2017)
- Freytes, J., Akkari, S., Dai, J., Gruson, F., Rault, P., Guillaud, X.: Small-signal state-space modeling of an HVDC link with modular multilevel converters. In: *IEEE 17th Workshop on Control and Modeling for Power Electronics (COMPEL)*, pp. 1–8. IEEE, Piscataway (2016)
- Akkari S.: Control of a multi-terminal HVDC (MTDC) system and study of the interactions between the MTDC and the AC grids. Ph.D. Thesis, Université Paris-Saclay (2016)
- Freytes, J., Akkari, S., Rault, P., et al.: Dynamic analysis of MMC-based MTDC grids: Use of MMC energy to improve voltage behavior. *IEEE Trans. Power Delivery* 34(1), 137–148 (2019). <https://doi.org/10.1109/TPWRD.2018.2868878>
- Small signal model of the studied MTDC system with F2F-MMC converter. [https://github.com/l2ep-cpmlab/VSC\\_Lib/tree/master/R2021a/Examples/IET\\_DCDC](https://github.com/l2ep-cpmlab/VSC_Lib/tree/master/R2021a/Examples/IET_DCDC)

**How to cite this article:** Shafique, G., Boukhenfouf, J., Gruson, F., Samimi, S., Colas, F., Guillaud, X.: Small signal analysis of DC voltage control based on a virtual resistance of DC/DC converter integrated in a multiterminal DC grid. *IET Gener. Transm. Distrib.* 1–14 (2024). <https://doi.org/10.1049/gtd.2.13262>

## APPENDIX

The cable parameters used in frequency dependent pi-model for small signal stability analysis are given below in Table A1 and the parameters for all MMC and F2F-MMC converters are presented in Table A2.

**TABLE A1** Cable parameters.

Parameter	Value	Parameter	Value
$R_{\zeta_1}$	0.0984 $\Omega$ /km	$L_{\zeta_1}$	0.1310 mH/km
$R_{\zeta_2}$	0.16560 $\Omega$ /km	$L_{\zeta_2}$	1.81570 mH/km
$R_{\zeta_3}$	0.0059 $\Omega$ /km	$L_{\zeta_3}$	3.1205 mH/km
$C_y$	0.241645 $\mu$ F/km	$G_y$	$0.607e^{-16}$ mho/km

**TABLE A2** MMC's and F2F-MMC parameters.

Parameter	Value
MMC's, F2F-MMC $R_{arm}$	0.05 $\Omega$
MMC's, F2F-MMC $L_{arm}$	48.94 mH
AC side resistance $R_g$	0.06 $\Omega$
AC side inductor $L_g$	60 mH
AC frequency	50 Hz
MMC's grid 1, F2F-MMC primary side MMC $C_{tot}$	195.31 $\mu$ F
MMC's grid 2, F2F-MMC secondary side MMC $C_{tot}$	320 $\mu$ F
Current controller (damping ratio $\zeta_i$ , time constant $\tau_i$ )	0.7, 1 ms
Energy controller (damping ratio $\zeta_W$ , time constant $\tau_W$ )	0.7, 50 ms